crystals

MDPI

Article

Fabrication and Characterization of Clay-Polyethylene Composite Opted for Shielding of Ionizing Radiation

S. F. Olukotun [1], S. T. Gbenu [2], K. O. Oyedotun [3], O. Fasakin [1,3], M. I. Sayyed [4,5,*], G. O. Akindoyin [6], H. O. Shittu [7], M. K. Fasasi [2], Mayeen Uddin Khandaker [8], Hamid Osman [9] and Basem H. Elesawy [10]

1 Department of Physics and Engineering Physics, Obafemi Awolowo University, Ile-Ife 220282, Nigeria; olukotunsf@oauife.edu.ng (S.F.O.); fasakinoladepo@gmail.com (O.F.)
2 Centre for Energy Research and Development (CERD), Obafemi Awolowo University, Ile-Ife 220282, Nigeria; sejlog@gmail.com (S.T.G.); mfasasi@oauife.edu.ng (M.K.F.)
3 Department of Physics, Institute of Applied Materials, University of Pretoria, Pretoria 0002, South Africa; kabir.oyedotun@up.ac.za
4 Department of Physics, Faculty of Science, Isra University, P.O. Box 7365, Amman, Jordan
5 Department of Nuclear Medicine Research, Institute for Research and Medical Consultations (IRMC), Imam Abdulrahman bin Faisal University (IAU), P.O. Box 1982, Dammam 31441, Saudi Arabia
6 Department of Chemistry, Obafemi Awolowo University, Ile-Ife 220282, Nigeria; akindoyingrace1@gmail.com
7 Department of Science Infrastructure, National Agency for Science and Engineering Infrastructure (NASENI), Abuja 900104, Nigeria; hammedshittu4luv@yahoo.com
8 Centre for Applied Physics and Radiation Technologies, School of Engineering and Technology, Sunway University, Bandar Sunway 47500, Malaysia; mayeenk@sunway.edu.my
9 Department of Radiology, College of Applied Medical Sciences, Taif University, Taif 21944, Saudi Arbia; ha.osman@tu.edu.sa
10 Department of Pathology, College of Medicine, Taif University, P.O. Box 11099, Taif 21944, Saudi Arabia; b.elesawy@tu.edu.sa
* Correspondence: mabualssayed@ut.edu.sa

Abstract: This study fabricated and characterized a self-sustaining hydrogenous content clay-polyethylene composite opted for ionizing radiation shielding. Composites designated A–G were fabricated each containing 0–30 wt% of recycled low density polyethylene (LDPE), respectively. To know the effects of the incorporated LDPE on the morphology, microstructural, compressive strength, thermal property and displacement effect on the vital elements were studied using scanning electron microscopy (SEM), X-ray diffractometry (XRD), universal mechanical testing machine, differential thermal analysis (DTA), Rutherford backscattering (RBS) technique and particle induced X-ray emission (PIXE), respectively. The bulk densities of the clay composites ranged between 1.341 and 2.030 g/cm^3. The samples' XRD analysis revealed similar patterns, with a sharp and prominent peak at angle 2θ equals ~26.11°, which matched with card number 16-0606 of the Joint Committee on Powder Diffraction Standards (JCPDS) that represents Aluminum Silicate Hydroxide ($Al_2Si_2O_5(OH)_4$), a basic formula for Kaolin clay. The compressive strength ranged between 2.52 and 5.53 MPa. The ratio of Si to Al in each composite is about 1:1. The dehydroxylation temperature for samples ranged between 443.23 °C and 555.23 °C.

Keywords: low density polyethylene (LDPE); clay composites; radiation shielding; XRD; PIXE

Citation: Olukotun, S.F.; Gbenu, S.T.; Oyedotun, K.O.; Fasakin, O.; Sayyed, M.I.; Akindoyin, G.O.; Shittu, H.O.; Fasasi, M.K.; Khandaker, M.U.; Osman, H.; et al. Fabrication and Characterization of Clay-Polyethylene Composite Opted for Shielding of Ionizing Radiation. *Crystals* **2021**, *11*, 1068. https://doi.org/10.3390/cryst11091068

Academic Editors: Georgy Lazorenko, Anton Kasprzhitskii and Zhaohui Li

Received: 3 August 2021
Accepted: 28 August 2021
Published: 3 September 2021

1. Introduction

In peaceful applications of nuclear technology, the inevitable emitted ionizing radiations need to be shielded to avert radiation exposure hazards. In radiation shielding design, gamma and fast neutrons are of more concern because they have highest penetrating power. The contributions of every gamma-matter physical interaction that can remove photons from a beam of gamma rays determine the gamma shielding capability of a material [1]. The probability of any interaction to occur is proportional to the atomic number (Z) *cum* density of the material the gamma ray is passing through. The parameters such as linear

attenuation coefficient (μ) and other parameters are often used to depict the gamma ray shielding ability of a material [2–4]. The mass attenuation coefficient of a composite material is summation of contributions of each element in the composite. It can be obtained using mixture rule (Bragg rule) given by Equation (1):

$$\left(\frac{\mu}{\rho}\right)_{mix} = \frac{\mu_1}{\rho_1}\omega_1 + \frac{\mu_2}{\rho_2}\omega_2 + \ldots = \sum_i \omega_i \left(\frac{\mu}{\rho}\right)_i, \quad (1)$$

where $\left(\frac{\mu}{\rho}\right)_i$ is element i mass attenuation coefficient. The weight fraction ω_i is given by

$$\omega_i = \frac{a_i A_i}{\sum a_j A_j} \quad (2)$$

Therefore, composite materials with high effective atomic number (Z_{eff}) are more effective for gamma shielding [5].

Furthermore, the probability of a particular interaction (either elastic or inelastic scattering) between an incident neutron and a target nucleus is usually expressed in term of microscopic cross section (σ). Macroscopic cross section, Σ (m^{-1}) is the product of the microscopic cross section σ (m^2) and atomic density N of the targeted material. For a composite material and a particular interaction, the macroscopic cross section is given by Equation (3) [6].

$$\Sigma(E) = \sum_i N_i \sigma_i(E) = \sum_i \frac{N_A}{A_i} \rho_i \sigma_i(E) \quad (3)$$

where N_i is the volumetric density of the ith nuclide, N_A is the Avogadro's number (6.023×10^{23}), while A_i and ρ_i are the partial density (g cm^{-3}) and atomic weight of the ith nuclide in the mixture respectively. The inverse of macroscopic cross sections gives average distance a neutron would travelled in a material before an interaction could occurred, and it is called mean free path (mfp) λ (m) [7,8]. From Equation (3), it is obvious that a light nucleus (such as hydrogen) would be more effective in fast neutron shielding.

In summary, high atomic number (Z) materials are needed to shield gamma ray, while low Z materials (especially hydrogenous materials) are needed for fast neutrons shielding. Therefore, a comprehensive radiation shielding system is made of either a multi-layers material or a composite material [6,9,10]. Studies have reported the ability of some composite materials such as clay and different kind of concretes for shielding of these ionizing radiations [8,11–14]. Furthermore, It has been revealed that this composites' fast neutron shielding capability depends on the amount of water content they retained. Therefore, the loss of water content in these composites is a huge weakness [8,15].

Studies have by Olukotun et al. (2018, 2019) [8,13] compared the gamma radiation shielding capability (GRSC) and fast-neutron shielding behaviour (FNSB) of clay with some existing shielding materials like iron and different kinds of concrete. Clay is composed of SiO_2, Al_2O_3 and water $(H_2O)n$ plus appreciable ccentration of iron, alkali and alkaline earth, and groups of crystalline substances known as clay minerals such as quatz, feldspar and mica [16]. It was observed that clay is good in gamma radiation shielding but its water content determines it fast neutron shielding capability. Its fast neutron shielding performance is enhanced with high water content. Kim et al. (2015) [15] pointed out that the loss of water content is a huge weakness of concrete in fast neutron shielding.

Clay-polyethylene, a self-sustaining hydrogeneous content composites named A–G which contained 0–30 respective wt% of recycled low density polyethylene (LDPE) were fabricated. The study revealed that the fast neutron shielding behaviour (FNSB) of the composite improved, while, its gamma rays shielding capability (GRSC) reduced as the wt% of LDPE increased in the matrix [17,18]. However, the effects of the incorporated LDPE on other required vital properties of clay such as microstructural, morphology, compressive strength and thermal property are yet to be reported. Numbers of materials' properties needed to withstand some stringent conditions such as high pressure, large thermal gradients and intense radiation are intimately related to their structures [19].

The aim of this study is to investigate the effects of the incorporated LDPE on the morphology, microstructural, compressive strength and thermal property on the clay matrix using scanning electron microscope (SEM) coupled with Energy dispersive X-ray Spectroscopy (EDX), X-ray diffraction (XRD), universal mechanical testing machine and differential thermal analysis (DTA), respectively. More also, details of the quantitative elemental compositions used to evaluate FNSB and GRSC of the composites [17,18] and displacement effect of the incorporated LDPE on some vital elements were also reported.

2. Materials and Methods

2.1. Preparation of the Clay Materials

The clay used was mined from Ladugbo, Ile-Ife, Osun State, Nigeria (7.49°N, 4.55°E). The clay lump form was crushed first to suitable sizes, sun-dried, and then pulverized. It was sieved with 2 mm sieve mesh.

2.2. Recycling and Processing of Waste Low Density Polyethylene

The low density polyethylene (LDPE) plastics are mostly used in Nigeria, West Africa for the packaging of water, popularly called sachet water. The LDPE plastic bags for the study were picked from pileups of waste sachet water bags. The bags were washed and shredded into pieces. They were dissolved in kerosene at 120 °C, to form a viscous liquid. The resulting slurry was quenched in an ice block chamber. After the cooling, acetone was used to remove kerosene content from the granulate substance. It was dried, pulverized and sieved to a particle size of less or equal to 2 mm [20].

2.3. Fabrication of Clay-Polyethylene Composite

The clay powder and the recycled LDPE granulate were blended. A laboratory mechanical mixer was used to achieve even distribution of LDPE in the clay matrix. This is briefly illustrated in Figure 1. Table 1 shows the mixing proportion in wt% of clay and LDPE. A 25ML amount of water was added, stirred and left for 24 h to get soaked. Each of the portions of the mixture was wedged to make it more pliable and remove any air bubbles. They were moulded and allowed to dry at room temperature for a few days until constant weight was achieved. The samples were further oven dried at relatively low temperature of about 100 °C for two hours to remove any left traces of water content.

Figure 1. Brief Illustration of LDPE recycling process and fabricated clay-polyethylene composites with different concentration of recycled LDPE.

Table 1. Mixing proportion of clay and LDPE.

Sample Name	wt% of Clay	wt% of LDPE
A	100	0
B	95	5
C	90	10
D	85	15
E	80	20
F	75	25
G	70	30

The bulk density of each of the samples was determined using boiling water method [21,22]. Each of the samples was transferred to a beaker filled with distilled water and boiled for 2 h in order to release the trapped air. It was allowed to cool and soak water. The suspended weight and saturated weight (which is free of excess water) were taken. The bulk density of each of the samples was then evaluated using the expression [23]:

$$Bulk\ Density = \frac{D}{w - S}\rho_w \tag{4}$$

where D, W, S and ρ_w are the sample dried weight, saturated weight, suspended weight and the water density, respectively.

2.4. Characterization of the Fabricated Clay-Polyethylene Composite

X-ray diffraction, scanning electron microscopy and Energy dispersive X-ray Spectroscopy were used to study the effects of the LDPE on the crystal structure of the clay matrix, the morphology and the qualitative elemental analysis of the fabricated composites, respectively. The ion beam techniques: Rutherford backscattering (RBS) and particle induced X-ray emission (PIXE) were used to investigate quantitative elemental composition of the composites. While the universal mechanical testing machine and differential thermal analysis (DTA) were used to investigate the compressive strength and the thermal properties of the fabricated clay-polyethylene composites, respectively.

i. X-ray diffraction (XRD)

The structural analyses of the samples were done within diffraction angle 2θ ranged from 0–60° using XPERT-PRO X-ray diffractometer (XRD) (PANalytical BV, Netherlands) located at the Department of Physics, Universityf Pretoria, South Africa. It is equipped with 25 kV high voltage source and a CuK_α radiation source of wavelength λ equal to 0.154 nm. XRD exploits dual nature (i.e., wave and particle) of X-rays using diffraction patterns to obtain information about the crystalline structure of materials [24]. The samples were grounded in to talc-like powder gently with friction to attain homogeneity and to also preserve their crystal structure. The samples were ground by 125 mL polypropylene grinding jar. Empty sample holders were filled with enough powder for each of the samples and gently pressed the powder flush with a glass slide. The surfaces of the powder were made smooth and carefully placed in the appropriate XRD slot. The generated monochromatic X-rays was collimated to concentrate and focused towards the sample. The interaction of the impinging monochromatic rays with the samples produced constructive interference (and diffracted ray) which condition satisfied the Bragg's law. Bragg's law is mathematically expressed as Equation (5) [25].

$$n\lambda = 2d\sin\theta \tag{5}$$

ii. Scanning electron microscope (SEM) coupled with Energy dispersive X-ray spectroscopy (EDX).

The morphology of each sample was studied using Zeiss Ultra plus 55 field emission scanning electron microscope (FESEM) (Carl Zeiss AG, Germany) at the Department of Physics, University of Pretoria, Hatfield, Pretoria, South Africa. The SEM and EDX are carried out on the same machine. The samples were cleaned ultrasonically using acetone, thoroughly degreased and dried to eliminate any outgassing from organic contamination and water. The samples being a non-conducting material were coated with a thin layer of carbon. Each of the samples was then mounted one after the other on the specimen holder. The technique focused beam of high-energy electrons to generate a variety of signals at the surface of the sample to create a magnified image of the sample [26]. The signals derived from electron-sample interactions revealed the external morphology and qualitative chemical composition of each sample. This entire process took place inside a

vacuum. The vacuum ensured that the electron beam interacts with the sample rather than the air.

iii. Stoichiometry elemental analysis of the fabricated composites

The 1.7 MV Tandem Pelletron Accelerator, Model 5SDH, by NEC, USA at the Centre for Energy Research and Development(CERD), Obafemi Awolowo University, Ile-Ife, Nigeria was used to obtain the quantitative elemental composition of the samples by employing PIXE and RBS techniques. The Ion Beam Analysis (IBA) facility is equipped with a RF charge ion source, equipped to provide proton and helium ions [27].

Each of the samples were pulverised using a washed mortar and pestle. Briquette of size 2 mm and 2 mm thick were made from the samples and loaded into the sample's holders at the End-station. Each sample was bombarded by 1.7 MV ion for 5 min. The qualitative and quantitative analysis of the elements in the samples were carried outusing GUPIXWIN and SIMNRA to analysis PIXE and RBS spectral, respectively.

iv. The compressive strength test

Universal Instron Machine (Model 3369) at the Centre for Energy Research and Development (CERD), Obafemi Awolowo University, Ile-Ife, Osun State, Nigeria was employed to test the compression strength of each sample. Cylindrical sample of 20 mm diameter and 20 mm height of each of the samples was placed on the load frame. The system crosshead was moved down to apply a compressive load on the sample. The load cell which is mounted in series with the sample, perceived the applied compressive load. This was converted into an electrical signal been measured and displayed by the control system. The compressive strength was obtained by Equation (6).

$$\text{Compressive Strength, } \sigma_c = \frac{F_q}{A_o} \text{ (Mpa)}, \tag{6}$$

where F_q was the force (load) at the onset of the sample failure and A_o was its initial cross sectional area.

v. Differential thermal analysis (DTA)

Every material experiences amount of internal heat generation whenever it is exposed in some severe environment. For instance, in a reactor environment, the primary source of the internal heat is due to gamma and neutron interaction with the material. In view of this, differential thermal analyzer (NETZSCH 4040PC) at the Centre for Energy Research and Development (CERD), Obafemi Awolowo University, Ile-Ife, Nigeria was used to study the thermal property of each sample.

The heat transition states of the samples were obtained by monitoring the temperature difference existing between each of the samples and a reference material, Al_2O_3 as a function of temperature (DTA). The same amount of each of the samples and the reference were put into the sample pan and reference pan, respectively. They were both subjected to the same heat from room temperature to 1200 °C. Theifference between the sample temperature and the reference temperature was plotted against the temperature to give information about the exothermic or endothermic transition that occurred in the sample.

3. Results

3.1. Bulk Density

The apparent densities of the fabricated composites are between 1.341 and 2.030 g/cm^3. The graph of the bulk density of the seven samples against the wt% of LDPE in the clay matrix is shown in Figure 2. Using the least square fit method, the relationship between the bulk density and percentage concentration of the LDPE is given by

$$\textit{Bulk Density}\left(\text{g cm}^{-3}\right) = 2.012 - 0.022 * (\%\ \textit{concentration of Recycled LDPE}). \tag{7}$$

The bulk density reduced linearly as the wt% of LDPE increased in the matrix. The trend is expected because LDPE has less density than clay. The obtained bulk density is in accordance with the earlier study by Aremu et al. [28].

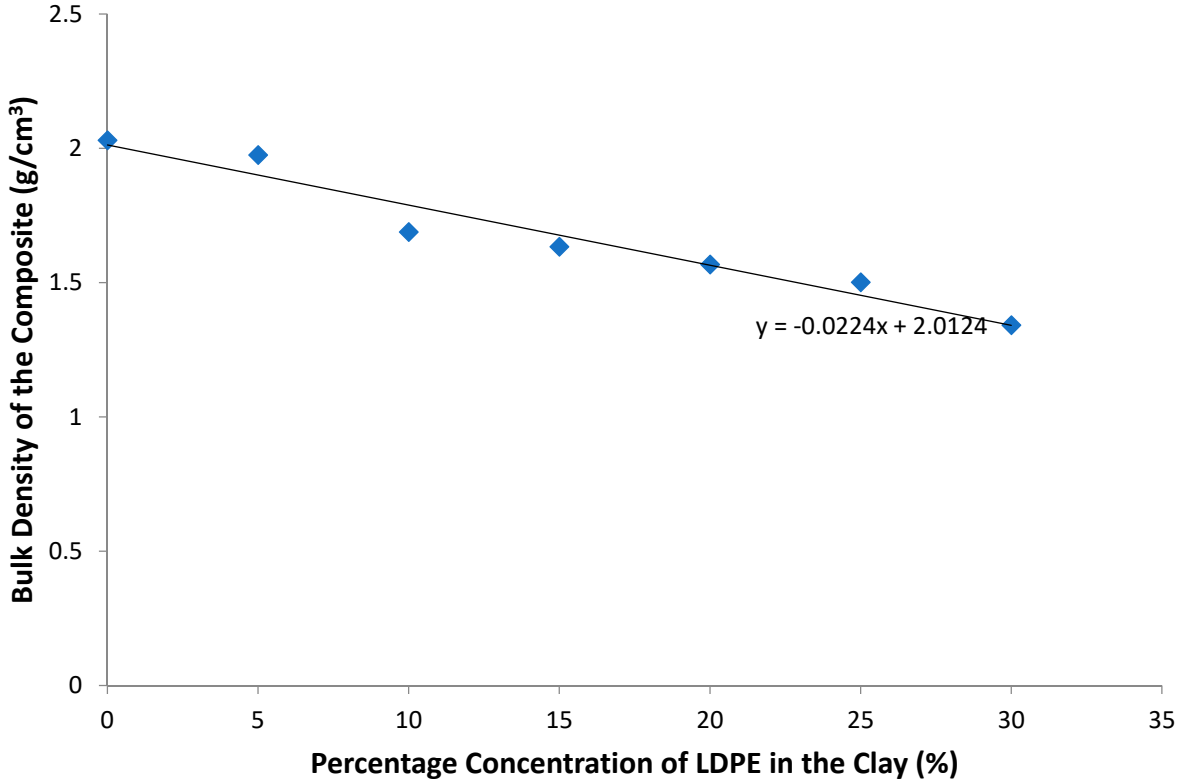

Figure 2. Variation of bulk density of the clay-polyethylene composites.

3.2. XRD Pattern of the Samples

Figure 3 depicts the XRD patterns of the studied Samples. From the pattern, reflections due to the samples are from the diffraction angle 2θ between 0 to 45°. The samples have a similar XRD pattern with one most prominent peak at diffraction angle 2θ equal to 26.11°. The XRD patterns show that clay is crystalline material, which is in line with the findings of other researchers such as Edah et al., Shen et al., Folorunso et al., and Ituma et al. [16,29–31]. The most prominent peak was analysed and it matched card number 16-0606 of the Joint Committee on Powder Diffraction Standards (JCPDS). The peak represents Aluminum Silicate Hydroxide ($Al_2Si_2O_5(OH)_4$), which is the basic formula for Kaolin clay.It was also noticed that as the concentration of LDPE increased in the clay matrix, the intensity of the most prominent peak reduced and became more broaden. This implies that the crystallinity of the clay reduced with increase in LDPE concentration.

3.3. SEM and EDX Results

The SEM micrographs of the samples, taken at the beam energy of 2 kV and scale of 1 µm with magnification range from 21.13 to 29.49 Kx, are shown in Figure 4a–g. The micrographs revealed densely packed agglomerate grains that are widely and evenly distributed across the clay matrix. The samples are less-porous in nature. It was noticed that LDPE concentration increased in the clay matrix the distinctiveness of the agglomerate grain boundaries are distorted and there appeared more of cluster bound grains. This implies that the crystallinity of the clay is reduced with an increasing of LDPE in the matrix. This is in agreement with what has been pointed out by the XRD spectral result.

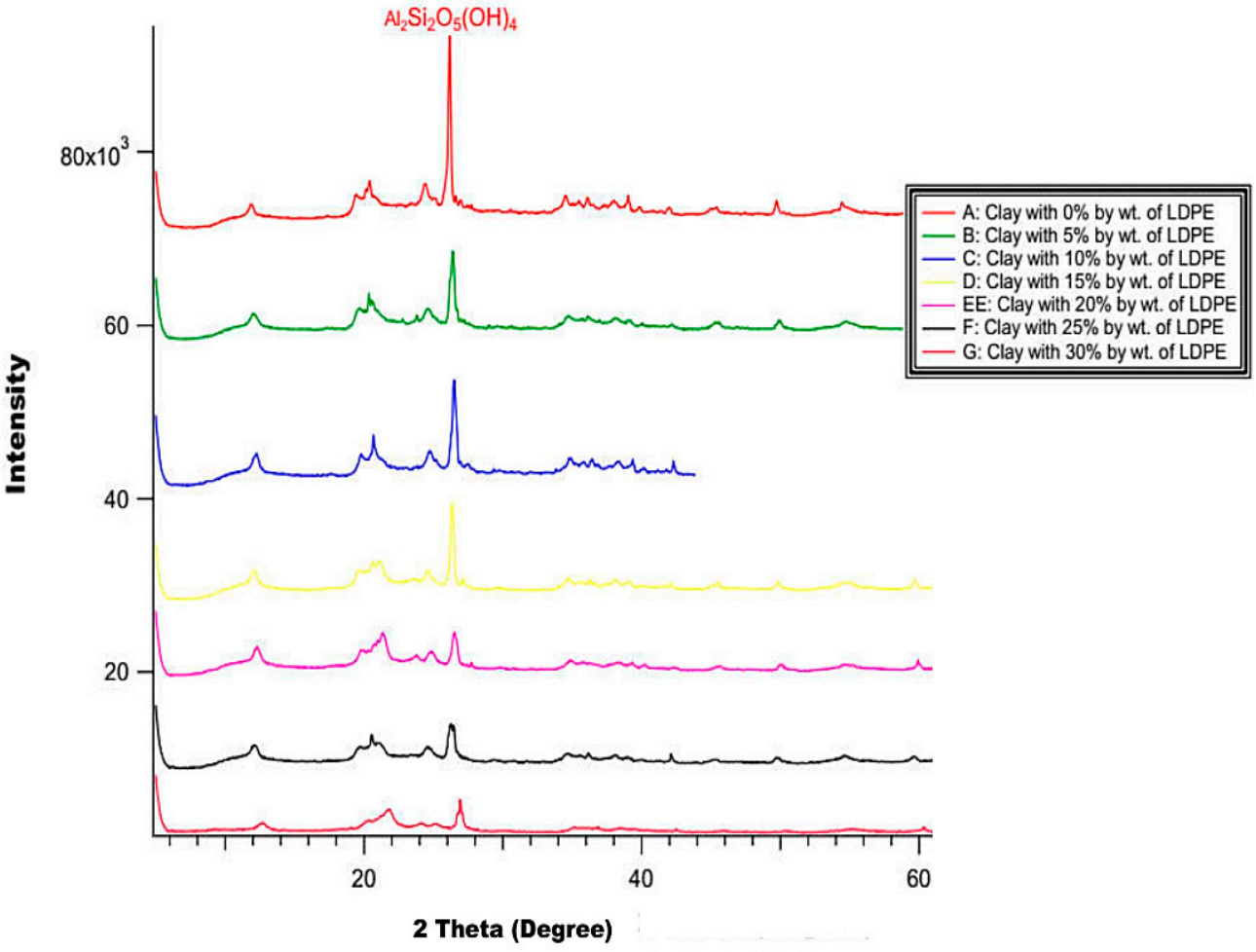

Figure 3. X-ray Diffraction (XRD) patterns of the studied Samples.

The EDX electron image, spectrum and elemental composition chats for Sample G is shown in Figure 5. The summary of the qualitative elemental composition of each of the samples in term of weight percent extracted each sample's elemental composition chats is given in Table 2. The proportions of the relative numbers of atoms (i.e., atomic fraction percent) for each element in the samples were obtained from the Table 2 and it is given in Table 3. The tables revealed that the major elements in the samples are C, O, Al, Si, Fe while the minor elements are Mg, K, and Ca. These major and minor elements were also identified by earlier studies by Wang et al., Er-ramly and Ider, Er-ramly, Abdullahi and Audu, Yahaya et al., Jiraskova et al. and Sokol et al. [32–38]

Oxygen is the most abundant element found in the samples with highest weight percent of 45.91 in sample A and the least value of 32.43 found in sample F. The next most abundant element is silicon, with highest value of 20.73 weight percent found in sample C, while the least value of 12.74 was found in sample E. The least abundant element found in the sample is Calcium (Ca) with the highest value of 0.41 weight percent found in sample G. The Tungsten (W) and Osmium (Os) were found only in sample D with value of 1.37 and 0.37 weight percent, respectively.

However, there is no specific quantitative trend noticed in the weight percent of the elements as the concentration of the LDPE increased in the clay matrix. This is because EDX is more of qualitative elemental analysis than quantitative analysis. This limitation was resolved by PIXE and RBS analysis results.

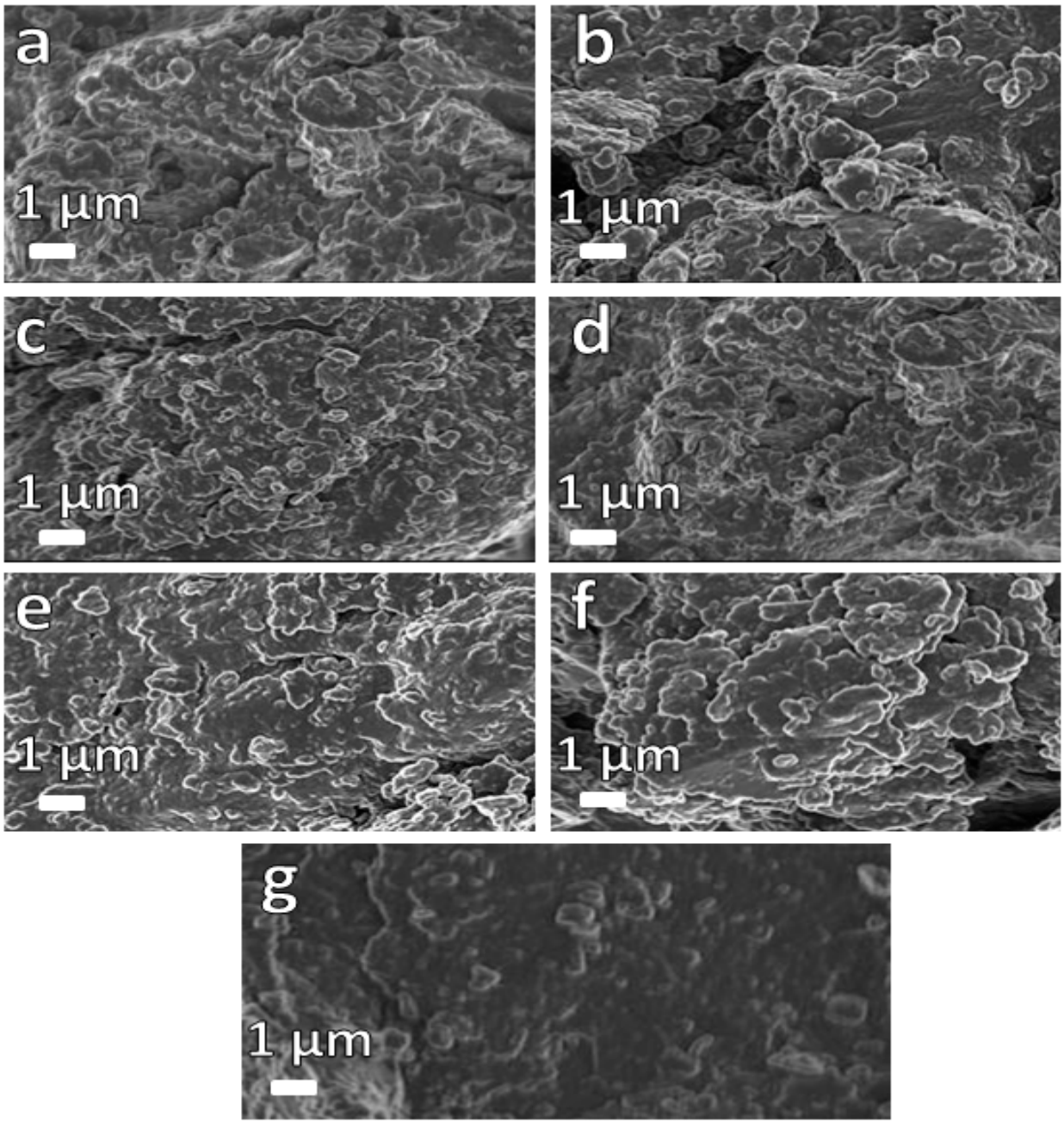

Figure 4. SEM Micrographs of the Sample: (**a**–**g**), respectively.

3.4. DTA and Compressive Strength Results

The DTA curves for each of the samples heated at the rate of 20 K/min to the temperature of 1200 °C are shown Figure 6. The dehydration and dehydroxylation transformations were noticed for all the samples. The dehydroxylation temperature for Sample A, B, C, D, E, F and G are 538.23 °C, 547.23 °C, 555.23 °C, 530.23 °C, 447.23 °C, 443.23 °C and 524.23 °C, respectively. These temperatures are pointed out with red arrows in Figure 6.The obtained temperatures are similar to those reported by earlier researchers such as Wang et al., Yeskis et al., Faieta-Boada and McColm, and Mukasa-Tebandeke et al. [32,39–41]. Each of these dehydroxylation temperatures is high enough to withstand any possible internal heat generation that could occur as a result of gamma rays and fast neutron interactions.

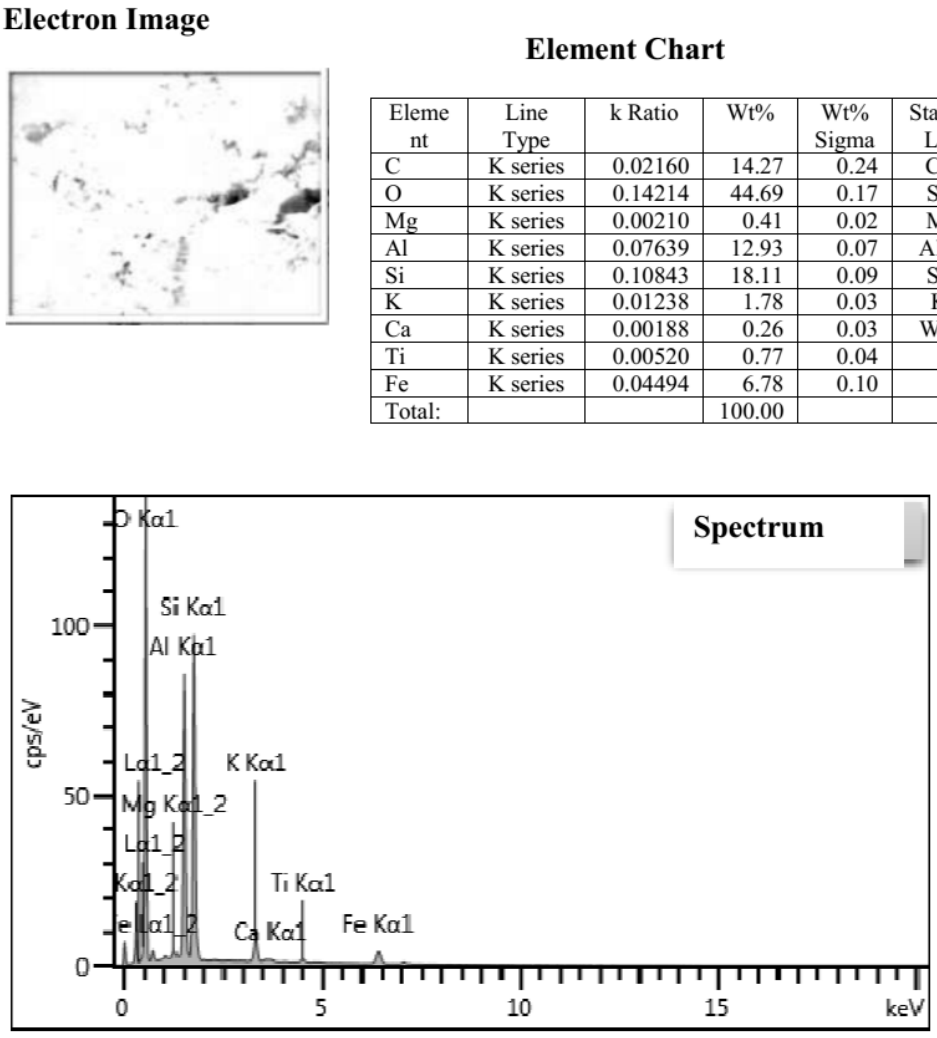

Element	Line Type	k Ratio	Wt%	Wt% Sigma	Standard Label
C	K series	0.02160	14.27	0.24	C Vit
O	K series	0.14214	44.69	0.17	SiO2
Mg	K series	0.00210	0.41	0.02	MgO
Al	K series	0.07639	12.93	0.07	Al2O3
Si	K series	0.10843	18.11	0.09	SiO2
K	K series	0.01238	1.78	0.03	KBr
Ca	K series	0.00188	0.26	0.03	Wolla.
Ti	K series	0.00520	0.77	0.04	Ti
Fe	K series	0.04494	6.78	0.10	Fe
Total:			100.00		

Figure 5. EDX electron image, spectrum and wt% (insets) of sample G.

Table 2. Summary of EDX elemental composition in Weight percent of the Samples.

	Sample A Bulk Density $\rho = 2.030$ g cm^{-3}		**Sample B Bulk Density** $\rho = 1.975$ g cm^{-3}		**Sample C Bulk Density** $\rho = 1.688$ g cm^{-3}		**Sample D Bulk Density** $\rho = 1.633$ g cm^{-3}		**Sample E Bulk Density** $\rho = 1.567$ g cm^{-3}		**Sample F Bulk Density** $\rho = 1.501$ g cm^{-3}		**Sample G Bulk Density** $\rho = 1.341$ g cm^{-3}	
Element	Wt%	Wt% Sigma	Wt%	Wt% Sigma	Wt%	Wt% Sigma	Wt%	Wt% Sigma	Wt%	Wt% Sigma	Wt%	Wt% Sigma	Wt%	Wt% Sigma
C	11.99	0.25	15.97	0.23	17.48	0.22	13.26	0.19	27.09	0.19	18.98	0.25	14.27	0.24
O	45.91	0.18	41.24	0.16	44.20	0.16	43.74	0.16	44.47	0.14	32.43	0.16	44.69	0.17
Mg	0.36	0.02	0.54	0.02	0.29	0.02	0.39	0.02	0.36	0.02	0.44	0.02	0.41	0.02
Al	13.81	0.07	12.35	0.06	9.78	0.05	12.48	0.06	9.51	0.05	11.33	0.07	12.93	0.07
Si	18.10	0.09	17.81	0.08	20.73	0.08	15.81	0.07	12.74	0.06	16.05	0.09	18.11	0.09
S	-	-	-	-	-	-	0.11	0.02	-	-	-	-	-	-
K	2.88	0.04	1.17	0.03	0.86	0.03	0.89	0.02	0.80	0.02	1.93	0.04	1.78	0.03
Ca	0.27	0.03	0.38	0.03	0.23	0.02	0.22	0.02	0.20	0.02	0.41	0.03	0.26	0.03
Ti	0.69	0.04	1.40	0.04	0.54	0.03	0.64	0.03	0.47	0.02	1.66	0.06	0.77	0.04
Fe	6.00	0.10	9.14	0.11	5.89	0.09	10.72	0.10	4.37	0.06	16.76	0.16	6.78	0.10
W	-	-	-	-	-	-	1.37	0.19	-	-	-	-	-	-
Os	-	-	-	-	-	-	0.37	0.09	-	-			-	-

Table 3. EDX elemental composition of the sample in weight percent and in atomic fraction percent.

	Sample A Bulk Density ρ = 2.030 g cm^{-3}		**Sample B Bulk Density** ρ = 1.975 g cm^{-3}		**Sample C Bulk Density** ρ = 1.688 g cm^{-3}		**Sample D Bulk Density** ρ = 1.633 g cm^{-3}		**Sample E Bulk Density** ρ = 1.567 g cm^{-3}		**Sample F Bulk Density** ρ = 1.501 g cm^{-3}		**Sample G Bulk Density** ρ = 1.341 g cm^{-3}	
Element	Wt%	Atomic Fraction%	Wt%	Atomic Fraction%	Wt%	Atomic Fraction%	Wt%	Atomic Fraction%	Wt%	Atomic Fraction%	Wt%	Atomic Fraction%	Wt%	Atomic Fraction%
C	11.99	19.05	15.97	25.32	17.48	26.59	13.26	21.55	27.09	37.80	18.98	31.55	14.27	22.38
O	45.91	54.72	41.24	49.04	44.20	50.43	43.74	53.31	44.47	46.54	32.43	40.43	44.69	52.56
Mg	0.36	0.29	0.54	0.43	0.29	0.22	0.39	0.32	0.36	0.25	0.44	0.37	0.41	0.32
Al	13.81	9.75	12.35	8.70	9.78	6.61	12.48	9.01	9.51	5.90	11.33	8.37	12.93	9.01
Si	18.10	12.33	17.81	12.10	20.73	13.51	15.81	11.01	12.74	7.62	16.05	11.43	18.11	12.17
S	-	-	-	-	-	-	0.11	0.07	-	-	-	-	-	-
K	2.88	1.41	1.17	0.57	0.86	0.40	0.89	0.45	0.80	0.34	1.93	0.99	1.78	0.86
Ca	0.27	0.13	0.38	0.18	0.23	0.10	0.22	0.11	0.20	0.08	0.41	0.20	0.26	0.12
Ti	0.69	0.27	1.40	0.55	0.54	0.21	0.64	0.26	0.47	0.16	1.66	0.69	0.77	0.30
Fe	6.00	2.04	9.14	3.11	5.89	1.92	10.72	3.73	4.37	1.31	16.76	5.97	6.78	2.28
W	-	-	-	-	-	-	1.37	0.15	-	-	-	-	-	-
Os	-	-	-	-	-	-	0.37	0.04	-	-	-	-	-	-

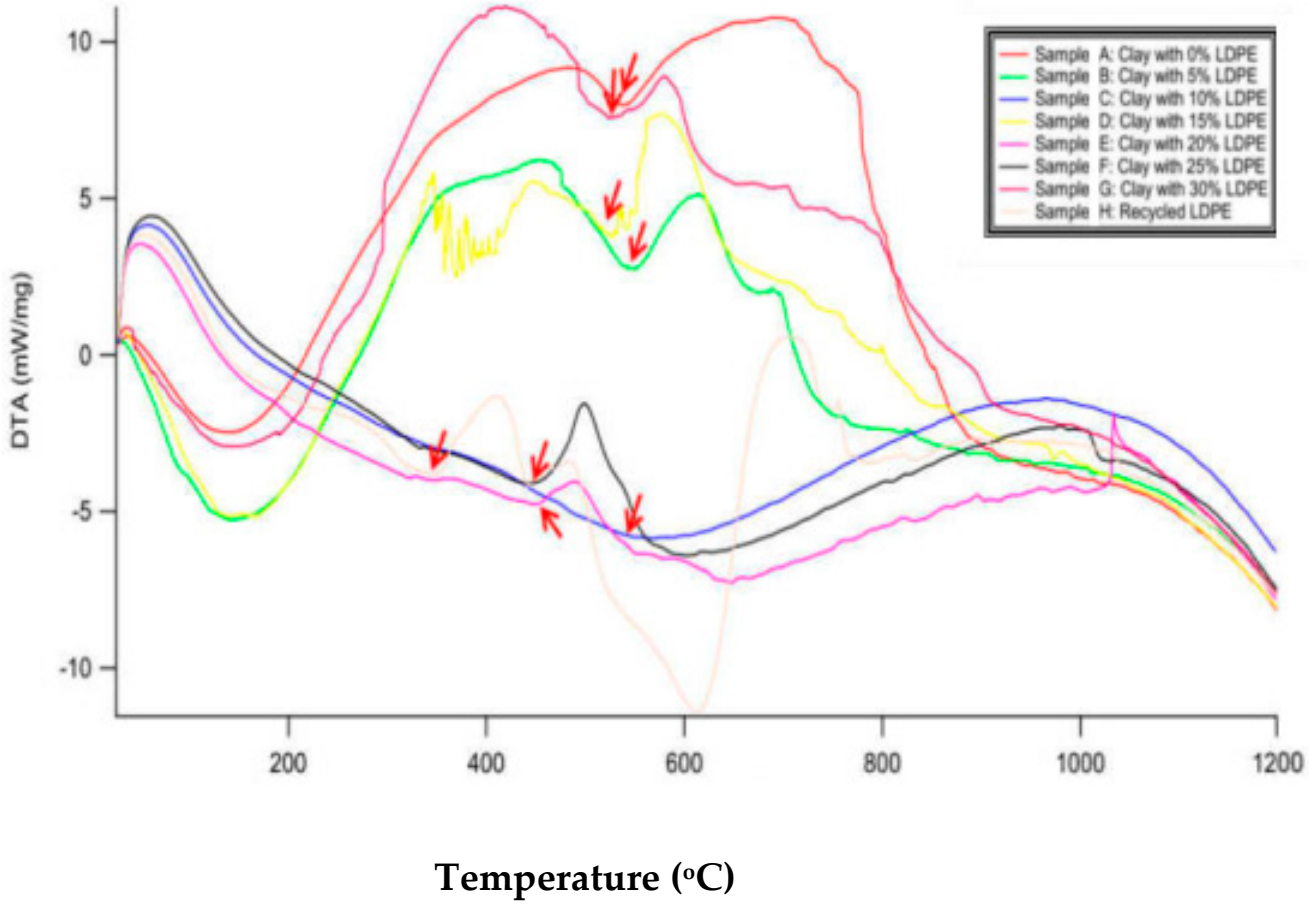

Figure 6. Differential thermal curves for the samples.

The compressive strength of each of the samples loaded to failure at a rate of 0.1 Ns^{-1} is shown in Figure 7. The obtained compressive strength of the samples ranged between 2.52 and 5.53 MPa. The compressive strength of the samples decreased as the concentration of LDPE increased in the clay matrix. This trend is similar to the findings of a earlier study and it implies that the ability of the samples to withstand direct pressure (load) is reducing as the LDPE concentration increases in the clay matrix [42].

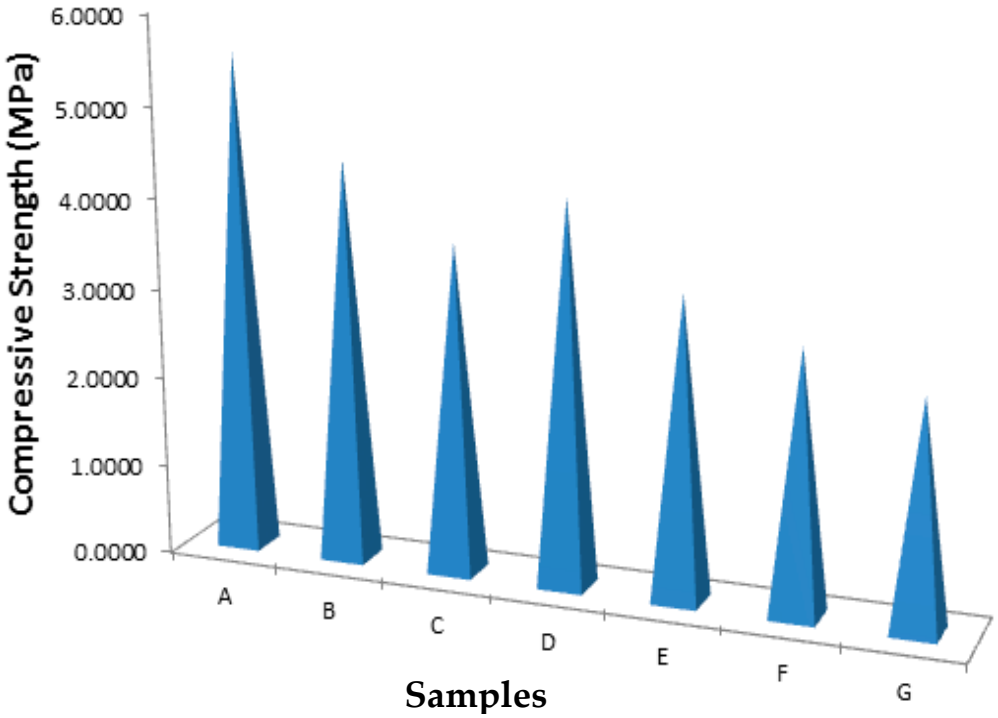

Figure 7. Compressive strength of the samples.

3.5. PIXE and RBS Results: Elemental Composition Analysis of the Samples

Table 4 gives the weight fraction of each element found in each of the composite samples (A–G) [17,18] and that of sample H which is the recycled LDPE. The major elements in the samples are C, Al, Si, Ca, and Fe while the minor elements are N, O, F, Mg, P, Cr, Mn, Zn, As, Sr and Zr. This is qualitatively the same with the EDX results presented earlier. The ratio of Si to Al for samples A–G is about 1:1. One of the earliest authors, Khandah et al. [43] on the properties of kaolin revealed that such ratio is peculiar to Kaolinite clay, which is crystalline in nature and thus confirms the results of XRD presented earlier. The elemental analysis of the recycled LDPE showed that the major elements are H, C, N, O and trace amount of F. This result is expected since LDPE is hydrocarbon.

The silicon and aluminum are the most abundant elements found in the composites, which agreed with the previous study [44]. The weight fraction of the silicon ranged between 0.2775 and 0.3964, and that of aluminum was between 0.2165 and 0.3092. This confirms what was obtained from the XRD results, which showed that the samples are Aluminum Silicate Hydroxide composites. Calcium, Tin and Iron are the most abundant high Z elements found in the samples. The weight fraction of calcium ranged between 0.0681 and 0.0972, 0.0160 and 0.0228 for Tin and Iron was between 0.0867 and 0.1239. It was observed that the weight fraction of these heavy elements decreased as the LDPE concentration increased in the clay matrix. This trend buttressed reasons why there was a decrease in the samples' bulk density as LDPE concentration is increasing in the clay matrix.

There is an increase in the weight fraction of Hydrogen and Carbon in the samples as the LDPE increases in the clay matrix. The weight fraction of Hydrogen ranged between 0.0067 and 0.0401, while for Carbon was between 0.0401 and 0.2408. The variation in Hydrogen and Carbon weight fraction in the samples and its effect on the weight fraction of the other major elements such as Si, Al and Fe are given in Figure 8. It was noticed that as weight fraction of Hydrogen and Carbon is increasing in the samples Si, Al and Fe weight fraction decreased proportionally. This would enhance the fast neutron shielding capability of the composite without depending on the amount of water retained.

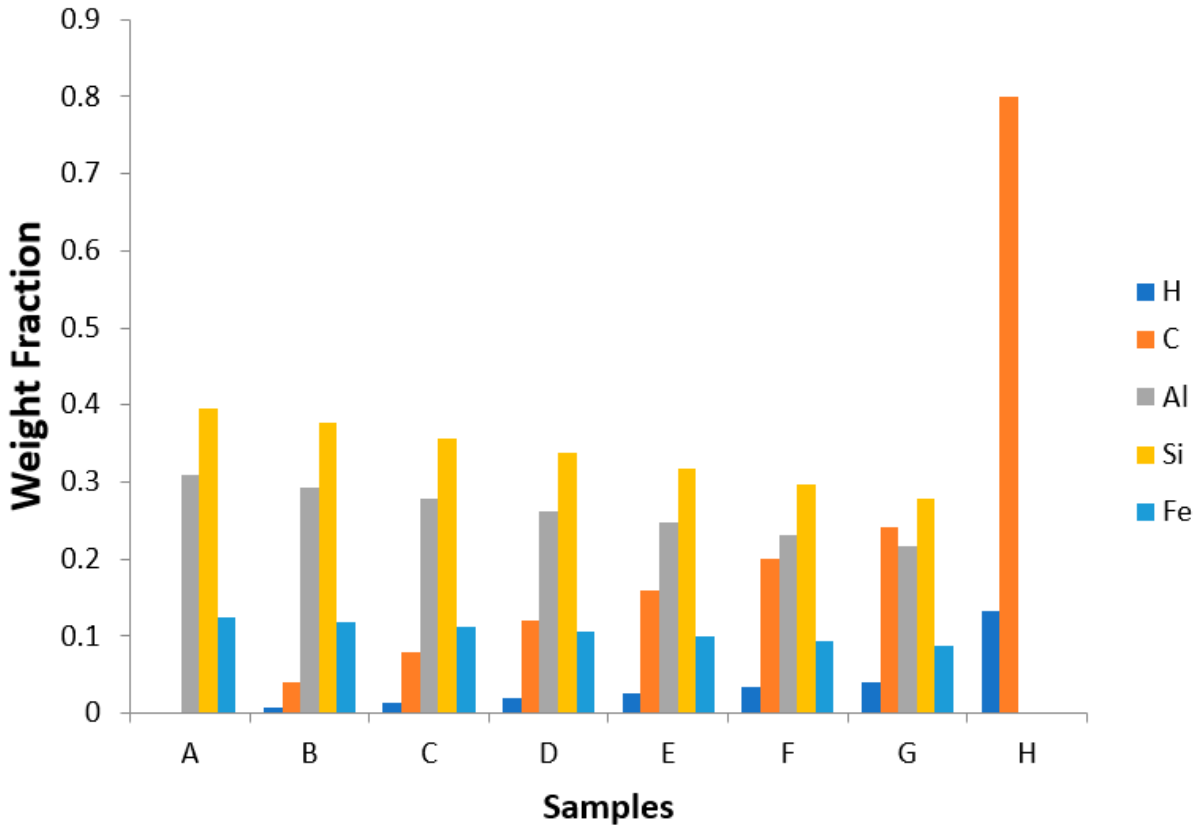

Figure 8. Variation of H, C, Al, Si and Fe weight fraction in the samples.

4. Conclusions

Clay-polyethylene composites composed of 0–30 wt% of recycled low density polyethylene (LDPE) were successfully fabricated. The effects of the incorporation of the recycled polymeric material into clay matrix were investigated by studying the microstructural, compressive strength, thermal property and elemental composition of the fabricated clay-polyethylene composites using X-ray diffraction (XRD), scanning electron microscope (SEM) coupled with energy dispersive X-ray Spectroscopy (EDX), instron universal testing machine, differential thermal analysis (DTA) and ion beam analysis techniques (PIXE and RBS). It was discovered that bulk density, crystallinity and compressive strength of the composites reduced as LDPE concentration increased in the clay matrix. The composite materials were observed to compose of C, Al, Si, Ca, and Fe as major elements, while the minor elements are N, O, F, Mg, P, Cr, Mn, Zn, As, Sr and Zr. It was observed that the weight fraction of Hydrogen and Carbon increased in the samples as LDPE concentration increased in the clay matrix. The dehydroxylation temperature for the composites ranged between 547.23 °C, and 443.23 °C.

The novelty of this study is that a self-sustaining hydrogenous content composite material—clay-polyethylene was successfully fabricated, which definitely have an enhanced fast neutron shielding behaviour. Concisely, the loss of water content would not be a concern if the composite is use for mixed radiation shielding.

The study also revealed that the amorphous low density polyethylene (LDPE) affected the crystallinity of the clay matrix. A study on the use of linear low density polyethylene (LLDPE) and high density polyethylene (HPE) that are crystalline in nature are recommended for further study. Such research would serve as basis for comparison and selection of better composite material for mixed-radiation shielding.

Table 4. The weight fraction of each element in the samples and density of each of the samples.

Element	H	C	N	O	F	Mg	Al	Si	P	K	Ca	Ti	Cr	Mn	Fe	Zn	As	Sr	Zr	Density g/cm^3
Sample A						0.0164	0.3092	0.3964	0.0013	0.0301	0.0972	0.0228	0.0006	0.0013	0.1239	0.0003	0.0001	0.0001	0.0003	**2.030**
B	0.0067	0.0401	0.0012	0.0020	0.0001	0.0156	0.2937	0.3766	0.0013	0.0286	0.0924	0.0217	0.0005	0.0012	0.1177	0.0003	0.0001	0.0001	0.0003	**1.975**
C	0.0133	0.0800	0.0025	0.0040	0.0002	0.0148	0.2784	0.3570	0.0012	0.0271	0.0875	0.0206	0.0005	0.0012	0.1115	0.0003	0.0000	0.0001	0.0003	**1.688**
D	0.0200	0.1202	0.0037	0.0060	0.0003	0.0140	0.2629	0.3370	0.0011	0.0256	0.0827	0.0194	0.0005	0.0011	0.1053	0.0003	0.0000	0.0001	0.0002	**1.633**
E	0.0267	0.1600	0.0049	0.0080	0.0004	0.0131	0.2474	0.3171	0.0011	0.0241	0.0778	0.0183	0.0004	0.0010	0.0991	0.0003	0.0000	0.0001	0.0002	**1.567**
F	0.0333	0.2001	0.0062	0.0100	0.0006	0.0123	0.2319	0.2973	0.0010	0.0226	0.0729	0.0171	0.0004	0.0010	0.0929	0.0003	0.0000	0.0001	0.0002	**1.501**
G	0.0401	0.2408	0.0074	0.0120	0.0007	0.0115	0.2165	0.2775	0.0009	0.0211	0.0681	0.0160	0.0004	0.0009	0.0867	0.0002	0.0000	0.0001	0.0002	**1.341**
H	0.1333	0.8000	0.0246	0.0399	0.0022															

Author Contributions: Conceptualization, S.F.O. and S.T.G.; methodology, K.O.O., G.O.A. and H.O.S.; software, O.F. and M.U.K. validation, M.I.S., M.K.F. and H.O.S.; formal analysis, S.F.O., K.O.O. and M.U.K.; investigation, S.F.O., O.F. and M.I.S.; writing—original draft preparation, S.F.O. and S.T.G. writing—review and editing, M.I.S., M.K.F. and O.F.; visualization, M.I.S.; supervision, M.K.F.; project administration, B.H.E.; funding acquisition, H.O. All authors have read and agreed to the published version of the manuscript.

Funding: We deeply acknowledge Taif University for supporting the researchers through Taif University Researchers Supporting Project number (TURSP-2020/127), Taif University, Taif, Saudi Arabia.

Institutional Review Board Statement: Not applicable.

Informed Consent Statement: Not applicable.

Data Availability Statement: The data presented in this study are available on request from thecorresponding author.

Acknowledgments: We would like to express our appreciation to the entire staff of Centre for Energy Research and Development (CERD), Obafemi Awolowo University, Ile-Ife and Department of Physical, University of Pretoria, Pretoria, South Africa for allowing us to use their facilities to characterize our samples. We want to express our profound gratitude to B. A. Tealeatu and B. Olofinjana of Department of Physics and Engineering Physics, Obafemi Awolowo University, Ile-Ife for support and guidance at various points of this work. The authors also acknowledge the support of Taif University Researchers Supporting Project number (TURSP-2020/127), Taif University, Taif, Saudi Arabia.

Conflicts of Interest: The authors declare no conflict of interest.

References

1. Robert, E.M. The Interaction of Radiation with Matter. In *Nuclear Engineering Fundamentals: A Practical Perspective*; CRC Press Taylor & Francis Group: Boca Raton, FL, USA, 2017; pp. 777–814.
2. Mostafa, A.M.A.; Issa, S.A.M.; Sayyed, M.I. Gamma ray shielding properties of PbO-B_2O_3-P_2O_5 doped with WO_3. *J. Alloys Compd.* **2017**, *708*, 294–300. [CrossRef]
3. Sayyed, M.I.; Al-Hadeethi, Y.; AlShammari, M.M.; Ahmed, M.; Al-Heniti, S.H.; Rammah, Y.S. Physical, optical and gamma radiation shielding competence of newly boro-tellurite based glasses: TeO_2-B_2O_3-ZnO-Li_2O_3-Bi_2O_3. *Ceram. Int.* **2021**, *47*, 611–618. [CrossRef]
4. Sayyed, M.I.; Askin, A.; Zaid, M.H.M.; Olukotun, S.F.; Khandaker, M.U.; Tishkevich, D.I.; Bradley, D.A. Radiation shielding and mechanical properties of Bi_2O_3-Na_2O-TiO_2-ZnO-TeO_2 glass system. *Radiat. Phys. Chem.* **2021**, *186*, 109556. [CrossRef]
5. Alallak, N.A.; Sarhan, S.S. Factors affecting gamma ray transmission. *Jordan J. Phys.* **2012**, *5*, 77–88.
6. Lamarsh, J.R.; Baratta, A.J. *Introduction to Nuclear Engineering*, 3rd ed.; Prentice Hall: Hoboken, NJ, USA, 2001.
7. Abd Elwahab, N.R.; Helal, N.; Mohamed, T.; Shahin, F.; Ali, F.M. New shielding composite paste for mixed fields of fast neutrons and gamma rays. *Mater. Chem. Phys.* **2019**, *233*, 249–253. [CrossRef]
8. Olukotun, S.F.; Mann, K.S.; Gbenu, S.T.; Ibitoye, F.I.; Oladejo, O.F.; Joshi, A.; Tekin, H.O.; Sayyed, M.I.; Fasasi, M.K.; Balogun, F.A.; et al. Neutron-shielding behaviour investigations of some clay-materials. *Nucl. Eng. Technol.* **2019**, *51*, 1444–1450. [CrossRef]
9. Tsoulfanidis, N. Computational Methods in Reactor Shielding. *Nucl. Technol.* **1984**, *64*, 102. [CrossRef]
10. Krane, K.S.; Lynch, W.G. *Introductory Nuclear Physics*, 3rd ed.; Physics Today; American Institute of Physics: New York, NY, USA, 1989. [CrossRef]
11. Akkurt, I.; El-Khayatt, A.M. The effect of barite proportion on neutron and gamma-ray shielding. *Ann. Nucl. Energy* **2013**, *51*, 5–9. [CrossRef]
12. Sayyed, M.I. Investigations of gamma ray and fast neutron shielding properties of tellurite glasses with different oxide compositions. *Can. J. Phys.* **2016**, *94*, 1133–1137. [CrossRef]
13. Olukotun, S.F.; Gbenu, S.T.; Ibitoye, F.I.; Oladejo, O.F.; Shittu, H.O.; Fasasi, M.K.; Balogun, F.A. Investigation of gamma radiation shielding capability of two clay materials. *Nucl. Eng. Technol.* **2018**, *50*, 957–962. [CrossRef]
14. Tajudin, S.M.; Sabri, A.H.A.; Aziz, M.Z.A.; Olukotun, S.F.; Ojo, B.M.; Fasasi, M.K. Feasibility of clay-shielding material for low-energy photons (Gamma/X). *Nucl. Eng. Technol.* **2019**, *51*, 1633–1637. [CrossRef]
15. Kim, J.D.; Ahn, S.; Lee, Y.D.; Park, C.J. Design optimization of radiation shielding structure for lead slowing-down spectrometer system. *Nucl. Eng. Technol.* **2015**, *47*, 380–387. [CrossRef]
16. Ituma, C.G.; Etukudoh, A.B.; Abuh, M.A.; Akpomie, K.G.; Obioha, C.I. Utilization of Nkpuma-Akpatakpa clay in ceramics: Characterization and microstructural studies. *J. Appl. Sci. Environ. Manag.* **2018**, *22*, 47–53. [CrossRef]

17. Olukotun, S.F.; Gbenu, S.T.; Oladejo, O.F.; Sayyed, M.I.; Tajudin, S.M.; Amosun, A.A.; Fadodun, O.G.; Fasasi, M.K. Investigation of gamma ray shielding capability of fabricated clay-polyethylene composites using EGS5, XCOM and Phy-X/PSD. *Radiat. Phys. Chem.* **2020**, *177*, 109079. [CrossRef]
18. Olukotun, S.F.; Gbenu, S.T.; Oladejo, O.F.; Balogun, F.O.; Sayyed, M.I.; Tajudin, S.M.; Obiajunwa, E.I.; Fasasi, M.K. The Effect of Incorporated Recycled Low Density Polyethylene (LDPE) on the Fast Neutron Shielding Behaviour (FNSB) of Clay Matrix using MCNP and PHITS Monte Carlo Codes. *Radiat. Phys. Chem.* **2021**, *182*, 109351. [CrossRef]
19. Callister, W.D.; Rethwisch, D.G. *Materials Science and Engineering—AnIntroduction*, 9th ed.; John Wiley and Sons Inc.: Hoboken, NJ, USA, 2013.
20. Azeko, S.T.; Mustapha, K.; Annan, E.; Odusanya, O.S.; Soboyejo, A.B.O.; Soboyejo, W.O. Statistical Distributions of the Strength and Fracture Toughness of Recycled Polyethylene-Reinforced Laterite Composites. *J. Mater. Civ. Eng.* **2016**, *28*, 04015146. [CrossRef]
21. ASTM C20. *Standard Test Methods for Apparent Porosity, Water Absorption, Apparent Specific Gravity, and Bulk Density of Burned Refractory Brick and Shapes by Boiling Water*; ASTM International: West Conshohocken, PA, USA, 2015; pp. 1–3. [CrossRef]
22. Chesti, A.R. *Refractories: Manufacture, Properties and Applications*; Prentice-Hall of India Private Ltd.: New Delhi, India, 1986.
23. Hassan, S.B. *Modern Refractories: Production, Properties, Testing and Application*; Timo Commercial Printers: Samaru, Zaria, 2005.
24. Satyanarayana, T. A Review on Chemical and Physical Synthesis Methods of Nanomaterials. *Int. J. Res. Appl. Sci. Eng. Technol.* **2018**, *6*, 2885–2889. [CrossRef]
25. Bouroushian, M.; Kosanovic, T. Characterization of Thin Films by Low Incidence X-Ray Diffraction. *Cryst. Struct. Theory Appl.* **2012**, *1*, 35–39. [CrossRef]
26. Danilatos, G.D. Review and outline of environmental SEM at present. *J. Microsc.* **1991**, *162*, 391–402. [CrossRef]
27. Obiajunwa, E.I.; Osinkolu, G.A.; Ibitoye, F.I.; Pelemo, D.A. Ion beam analysis facility at the centre for energy research & development at Ile-Ife Nigeria and its applications in research. *Nucl. Instrum. Methods Phys. Res. Sect. B Beam Interact. Mater. Atoms.* **2019**, *477*, 46–53. [CrossRef]
28. Aremu, D.A.; Aremu, J.O.; Ibrahim, U.H. Analysis Of Mubi Clay Deposit As A Furnace Lining. *Int. J. Sci. Technol. Res.* **2013**, *2*, 182–186.
29. Edah, A.O.; Kolawole, J.A.; Solomon, A.O.; Shamle, N.; Awode, A.U. Instrumental analysis of Arrinrasho clay for characterization. *J. Res. Environ. Sci. Toxicol.* **2012**, *1*, 019–022.
30. Shen, S.; Zaidi, S.R.; Mutairi, B.A.; Shehry, A.A.; Sitepu, H.; Hamoud, S.A.; Khaldi, F.S.; Edhaim, F.A. Quantitative XRD bulk and clay mineralogical determination of paleosol sections of Unayzah and Basal Khuffclastics in Saudi Arabia. *Powder Diffr.* **2012**, *27*, 126–130. [CrossRef]
31. Folorunso, D.O.; Olubambi, P.; Borode, J.O. Characterization and Qualitative Analysis of Some Nigerian Clay Deposits for Rafractory Applications. *IOSR J. Appl. Chem.* **2014**, *7*, 40–47. [CrossRef]
32. Wang, H.; Li, C.; Peng, Z.; Zhang, S. Characterization and thermal behavior of kaolin. *J. Therm. Anal. Calorim.* **2011**, *105*, 157–160. [CrossRef]
33. Er-ramly, A.; Ider, A. Physicochemical and mineralogical characterization of grey clay resulting from the transformation of brown clay of Safi treated with (HCL) and its use in ceramic. *Phys. Chem. News* **2012**, *66*, 100–106.
34. Er-ramly, A. Physicochemical and Mineralogical Characterization of Moroccan Bentonite of Trebia and Its Use in Ceramic Technology. *Am. J. Phys. Chem.* **2014**, *3*, 96–101. [CrossRef]
35. Abdullahi, S.L.; Audu, A.A. Comparative analysis on chemical composition of bentonite clays obtained from Ashaka and tango deposits in Gombe State, Nigeria. *ChemSearch J.* **2017**, *8*, 35–40.
36. Yahaya, S.; Jikan, S.S.; Badarulzaman, N.A.; Adamu, A.D. Effects of Acid Treatment on the SEM-EDX Characteristics of Kaolin Clay. *Path Sci.* **2017**, *3*, 4001–4005. [CrossRef]
37. Jiraskova, Y.; Bursik, J.; Seidlerova, J.; Kutlakova, K.M.; Safarik, I.; Safarikova, M.; Pospiskova, K.; Zivotsky, O. Microstructural analysis and magnetic characterization of native and magnetically modified montmorillonite and vermiculite. *J. Nanomater.* **2018**, *2018*, 3738106. [CrossRef]
38. Sokol, H.; Sprynskyy, M.; Ganzyuk, A.; Raks, V.; Buszewski, B. Structural, Mineral and Elemental Composition Features of Iron-Rich Saponite Clay from Tashkiv Deposit (Ukraine). *Colloids Interfaces* **2019**, *3*, 10. [CrossRef]
39. Yeskis, D.; Van Groos, A.F.K.; Guggenheim, S. The dehydroxylation of kaolinite. *Am. Mineral.* **1985**, *70*, 159–164.
40. Faieta-Boada, S.M.; McColm, I.J. Preliminary analysis of the thermal behaviour of an industrially used Ecuadorian clay. *Appl. Clay Sci.* **1993**, *8*, 215–230. [CrossRef]
41. Mukasa-Tebandeke, I.Z.; Ssebuwufu, P.J.M.; Nyanzi, S.A.; Schumann, A.; Nyakairu, G.W.A.; Ntale, M.; Lugolobi, F. The Elemental, Mineralogical, IR, DTA and XRD Analyses Characterized Clays and Clay Minerals of Central and Eastern Uganda. *Adv. Mater. Phys. Chem.* **2015**, *5*, 67–86. [CrossRef]
42. Quaranta, N.; Caligaris, M.; Unsen, M.; López, H.; Pelozo, G.; Pasquini, J.; Vieira, C. Ceramic Tiles Obtained from Clay Mixtures with the Addition of Diverse Metallurgical Wastes. *J. Mater. Sci. Chem. Eng.* **2014**, *2*, 1–5. [CrossRef]
43. Khandah, R.K.; Gangopadhyay, P.K.; Rao, T.C. *Differential Thermal Analysis of Studies of some Indian Clays*; Proc. Indian Natn. Sci. Acad. Clay Science: Calcutta, India, 1984; pp. 234–241.
44. Omotoyinbo, J.A.; Oluwole, O.O. Working Properties of Some Selected Refractory Clay Deposits in South Western Nigeria. *J. Miner. Mater. Charact. Eng.* **2008**, *7*, 233–245. [CrossRef]